I&EC research
Industrial & Engineering Chemistry Research
pubs.acs.org/IECR
Article

Comparative Effects on Recrystallization of Melt-Memory and Liquid−Liquid Phase Separation in Ziegler−Natta and Metallocene Ethylene Copolymers with Bimodal Comonomer Composition Distribution

Minqiao Ren, Xuejian Chen, Yuan Sang, and Rufina G. Alamo*

Cite This: *Ind. Eng. Chem. Res.* 2020, 59, 19260−19271
Read Online
ACCESS | Metrics & More | Article Recommendations | Supporting Information

ABSTRACT: Herein, we study comparatively melt-memory effects on recrystallization of two sets of linear low-density polyethylenes (LLDPE) synthesized with Ziegler−Natta (ZN-LLDPE) and with metallocene catalysts (M-LLDPE), respectively. All copolymers have $M_w \sim 120{,}000$ g/mol, $M_w/M_n \sim 4$, and very similar average comonomer content (~2 mol % branches) but different comonomer composition distribution (CCD). While all types of copolymers display the strong melt-memory effect of the initial crystallites enhancing the recrystallization rate from melt temperatures (T_{melt}) up to ~160 °C, a subsequent retardation of the rate associated with liquid−liquid phase separation (LLPS) is found mainly in ZN-LLDPEs. Only one M-LLDPE displays the retardation of the recrystallization rate. The conclusion from a detailed quantitative analysis of the TREF profiles is that copolymers with inversion of crystallization rate, characteristic of LLPS, have CCD comprising 15−25 wt % molecules in the 12−6 mol % comonomer range and <50 wt % in the 6−1.5 mol % comonomer range. The rest (30−50 wt %) are lowly branched molecules (<1.5 mol %) that comprise the high-crystallinity component. Characterization of the spherulitic crystalline morphology with polarized optical microscopy allows us to extract the exponential variation of the number of residual clusters (self-nuclei) in the melt as a function of decreasing T_{melt} within the melt-memory range. The comparative CCD-crystallization analysis carried out in this work serves as a guideline to design LLDPEs with distributions prone to LLPS during processing.

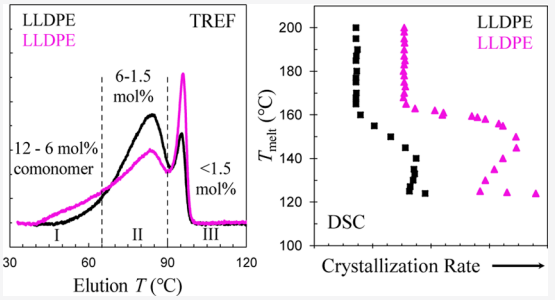

1. INTRODUCTION

Commercial linear low-density polyethylenes (LLDPEs) are random copolymers of ethylene and an α-olefin incorporated at levels between 2 and 15 mol %. Typical α-olefin comonomer units are 1-butene, 1-hexene, and 1-octene. The commercial copolymerization is carried out using Ziegler−Natta (ZN) or metallocene (M) catalysts in homogeneous or heterogeneous processes. Copolymers produced with Ziegler−Natta catalysts display broad molecular weight distribution (MWD) and bimodal interchain comonomer composition distribution (CCD), with the highest comonomer content accumulated in the low-molecular-weight chains.[1−9] Conversely, single-site metallocene catalysts lead to narrow MWD and narrow interchain CCD. Metallocene catalysts are also modified to produce LLDPE resins with single MWD or with bimodal MWD and a preferred incorporation of comonomer in the longest chains for a superior process/property balance.[3,4] It is perceived that the placement of comonomer in the high molar mass portion of the distribution increases the chain connectivity between crystallites (tie chains). Such metallocene LLDPEs with bimodal but orthogonal comonomer composition distribution (BOCCD) have enhanced tear and dart impact compared to classical ZN copolymers.[6,9]

The mechanical properties of LLDPEs are a function of the semicrystalline structure developed during processing; therefore, understanding the state of the melt and crystallization of ZN and M-LLDPEs with comparable bimodal interchain CCD is important for a better control of the ultimate properties of these materials via tuning the chemical microstructures.

Recently, we discovered that melts of random ethylene copolymers display a strong memory of the previous crystalline state up to temperatures ~65 °C above their observed final melting, and ~30° above their equilibrium melting point.[10−18] When crystalline LLDPEs are heated to temperatures above the observed melting, but within the range of melt memory, the recrystallization kinetics is significantly enhanced. This

Received: July 27, 2020
Revised: September 28, 2020
Accepted: September 30, 2020
Published: September 30, 2020

https://dx.doi.org/10.1021/acs.iecr.0c03647
Ind. Eng. Chem. Res. 2020, 59, 19260−19271

Table 1. Characterization of Ethylene Copolymers Synthesized with ZN Catalysts

sample ID	comonomer type	average branching content (mol %)	M_w (g/mol)	M_w/M_n	T_m (°C)	ΔH (J/g)
ZN EH1.7	1-hexene	1.7	120 000	4.0	124.3	121.4
ZN EH1.9	1-hexene	1.9	110 000	4.7	124.1	93.2
ZN EB2.1	1-butene	2.1	112 000	3.9	121.0	113.8
ZN EO2.0	1-octene	2.0	122 000	4.5	120.8	116.7
ZN EO2.2	1-octene	2.2	130 000	4.8	119.1	112.7

remarkable effect is attributed to molten clusters of ethylene sequences that compose the initial crystals. These molten sequences remain in close proximity (retain space memory) well above the crystal melting. On recrystallization, such clusters act as self-nuclei lowering or bypassing the usually high energy barrier for nucleation, hence speeding up the crystallization process.

Beyond the academic drive to understand the crystallization of polymers, there is industrial interest in this peculiar self-nucleation. As commercial crystalline polymers are processed from the melt, recrystallization from self-nucleated melts (those in the melt-memory range) can shorten molding or solidification cycles with obvious commercial profits. Faster recrystallization also improves the optical properties of films, such as transparency and haze, by reducing the size of the spherulites due to enhanced nucleation density.

The strong melt memory of LLDPEs is attributed to the formation of a topologically complex amorphous region during sequence partitioning in the LLDPE crystallization process.[10,12] Since branches longer than methyl are excluded from the crystals, during LLDPE crystallization, suitable ethylene sequences have to diffuse to the crystal front. On the path to crystallization, branches, knots, loops, and other topological constraints are rejected to the intercrystalline regions, especially at high levels of transformation, and accumulate preferentially at the basal surface of the lamellar crystallites. It is perceived that on melting, diffusion of crystalline sequences to a randomized melt is hampered by the constraints in the amorphous regions and requires temperatures well above the equilibrium melting point.[10,12,17,18] The fact that both molecular weight and level of crystallinity affect the strength of melt memory, and that there exist threshold values below which melt memory vanishes, supports the diffusion-limited rationale posited to explain the strong melt memory observed in LLDPEs.[10,12,17] Unbranched polyethylenes do not display strong melt memory.[10]

In a subsequent work, we compared the effect of melt memory on crystallization of narrowly and two broadly distributed commercial LLDPEs[13] and found a remarkable behavior of the latter. The narrow LLDPEs displayed a strong memory of crystallization and enhanced recrystallization rates from temperatures (T_{melt}) above the equilibrium melting point akin to the behavior of model ethylene 1-butene random copolymers.[13] The recrystallization of two LLDPEs with a broad CCD ranging from 0.5 to 13 mol % comonomer showed an additional feature. When cooled from very high-melt temperatures, these copolymers displayed first a constant recrystallization range, followed by accelerated crystallization with lowering T_{melt} as is observed in the narrow resins. With a further decrease of T_{melt}, between ∼150 and ∼125 °C, there was an unexpected decrease of the recrystallization rate in the broad copolymers. This inversion of the recrystallization rate was explained as demarcating the onset of liquid−liquid phase separation (LLPS) between comonomer-rich and comonomer-poor molecules.[13] The decrease of the recrystallization rate with lowering T_{melt} in the LLPS region is a consequence of a decrease in number of clusters due to the strong thermodynamic drive for molecular segregation between molecules with a difference in comonomer content >8 mol %. In crossing the LLPS binodal line, there is rapid diffusion of the crystalline sequences toward equilibrating the composition of the two liquid phases and thus effectively dissolving self-nuclei. The LLPS of the broadly distributed copolymer was further confirmed by direct measurements of the state of the melt using neutron scattering experiments.[14]

A feature of interest of the reversed dependence of the crystallization rate on the decreasing melt temperature of copolymers with broad CCD is the simplicity of the experiment to characterize the state of the melt and its potential effect to enhance the impact properties of LLDPEs with specific CCD distributions.[6,13] Preliminary studies with ZN copolymers indicate an effect of the content of molecules across the CCD distribution on the extent of melt memory and liquid−liquid phase separation of ZN-LLDPE.[16] Of interest are the threshold contents of molecules with a difference in comonomer content higher than 6−8 mol % to observe LLPS behavior by the reverse effect on crystallization from melts with memory. In the present work, we quantify the content of molecules in different regions of the CCD and correlate these data with the extent of melt memory and LLPS in a larger set of commercial ZN copolymers. Furthermore, the same analysis is conducted in a set of bimodal broadly distributed metallocene copolymers. To minimize the effects of molecular characterization other than that of the interchain CCD, the LLDPEs synthesized with ZN catalysts and with metallocene catalysts feature similar molar mass, similar molar mass distribution, and almost the same average comonomer content. Details of the distribution that allow a clear signature of LLPS are highlighted. We also provide direct evidence of self-nuclei during recrystallization from melts with crystalline memory.

2. EXPERIMENTAL SECTION

2.1. Materials. Two sets of samples were used in this study. The first set is commercial ethylene copolymers with broad-bimodal CCD synthesized with ZN catalysts. The average molecular mass and branching content are listed in Table 1. The ethylene 1-hexene copolymer designated as ZN EH1.7 was provided by ExxonMobil Co. and was used in a previous work.[19] It was demonstrated by neutron scattering that ZN EH 1.7 contains a small fraction of highly branched molecules that phase-separate in the melt.[19] ZN EH1.9 and ZN EB2.1 are ethylene 1-hexene and ethylene 1-butene copolymers, respectively, and were provided by Sinopec Co. The other two ethylene 1-octene copolymers, ZN EO2.2 and ZN EO2.0, are manufactured by Dow Chemical Co.

The second set includes ethylene copolymers with bimodal CCD synthesized with metallocene catalysts. Their average molecular mass and average branching content are listed in

https://dx.doi.org/10.1021/acs.iecr.0c03647
Ind. Eng. Chem. Res. 2020, 59, 19260−19271

Table 2. Characterization of Ethylene Copolymers Synthesized with Metallocene Catalysts

sample ID	comonomer type	average branching content (mol %)	M_w (g/mol)	M_w/M_n	T_m (°C)	ΔH (J/g)
M EH1.2	1-hexene	1.2	110 000	2.7	116.8	107.1
M EH1.3	1-hexene	1.3	125 000	3.0	119.5	108.7
M EO1.3	1-octene	1.3	128 000	4.4	119.3	93.4
M EO1.4	1-octene	1.4	107 000	3.9	120.6	110.0
M EH1.7	1-hexene	1.7	123 000	3.6	121.3	107.6

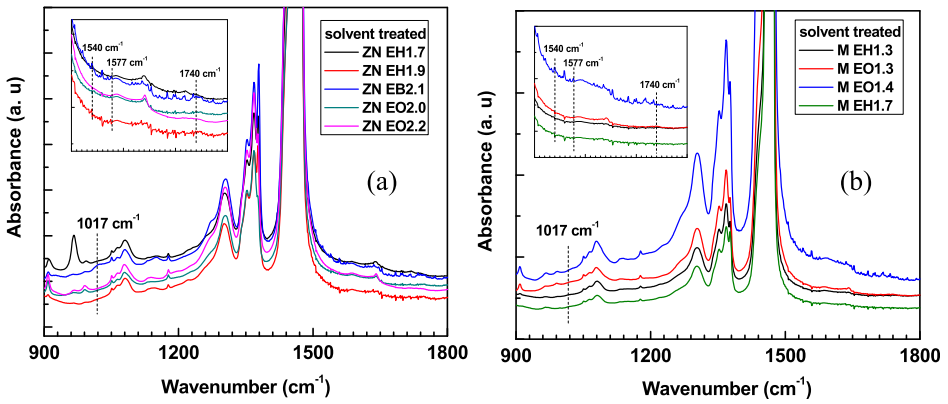

Figure 1. Room-temperature FTIR spectra of solvent treated (a) ZN-LLDPEs and (b) M-LLDPEs.

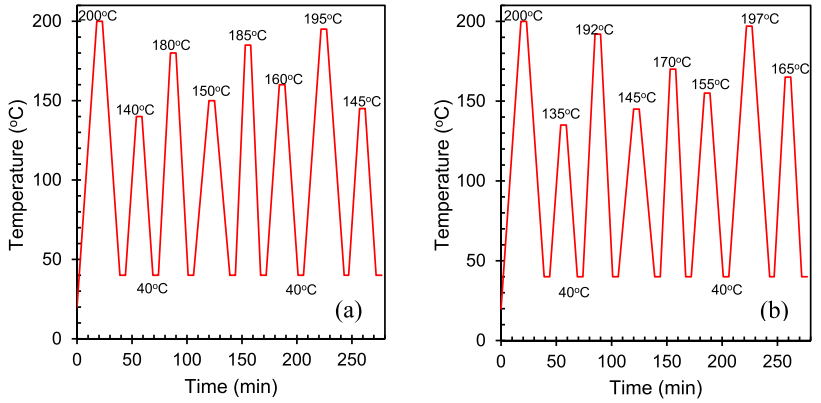

Figure 2. Representative heating and cooling profiles for crystallizations from different initial melting temperatures. Each copolymer was subjected to three cycles, to cover a large range of T_{melt}. (a) and (b) show two of these cycles. Heating and cooling rates are both 10 °C/min. Holding time at each temperature is 5 min.

Table 2. As shown, the average comonomer content and molecular mass are very similar to the ZN copolymers. Ethylene 1-hexene copolymers M EH1.2 and M EH1.3 were provided by Sinopec Co. M EH1.3 is a commercial resin, while M EH1.2 is an experimental laboratory specimen. Ethylene 1-octene copolymers M EO1.3 and M EO1.4 were provided by Dow Chemical Co., and ethylene 1-hexene copolymer M EH1.7 was provided by ExxonMobil Co. All GPCs can be found in Figure S1.

Except for M EH1.2 that was received as reactor powder, all ZN and metallocene LLDPEs were received as pellets. The molecular mass and polydispersity index were analyzed by GPC using polyethylene standards, and the average branching content by ^{13}C NMR.[20] Tables 1 and 2 also list the peak melting temperatures and heats of fusion of all copolymers crystallized by cooling from 200 °C at 10 °C/min to 40 °C.

2.2. Methods and Techniques. Prior to DSC and microscopy analysis of the melt-memory behavior, all of the copolymers except M EH1.2 were recrystallized from a 0.01% w/v solution in xylene at 120 °C using cold acetone as the polymer precipitant. Since acetone is miscible with xylene and is a good solvent at room temperature for the most common antioxidants, such as Irganox and Irgafos, these and other additives that may interfere with the copolymer's melt memory remain dissolved in acetone and are separated from the polymer after filtration. Talc, an effective nucleant, was also removed quantitatively from ZN EH1.7 using Soxhlet extraction following the procedure described previously.[13] The presence of Irganox, calcium stearate, and talc prior to and removal after solvent treatment was evaluated by transmission FTIR using a Thermo Scientific Nicolet 6700 spectrometer equipped with a TE cooled DTGS detector. The spectral range was 400−4000 cm^{-1} and the resolution was 2 cm^{-1}. The molecular weight prior to and after solvent treatment is unchanged (Figure S2).

Figure 1a,b shows FTIR spectra of the solvent-treated or Soxhlet-extracted ZN-LLDPEs and M-LLDPEs, respectively. The absorption characteristic of the Si−O−Si asymmetric stretching vibration of talc at 1017 cm^{-1} that was present in the spectra of the original ZN EH1.7 and M EO1.3 copolymers is

https://dx.doi.org/10.1021/acs.iecr.0c03647
Ind. Eng. Chem. Res. 2020, 59, 19260−19271

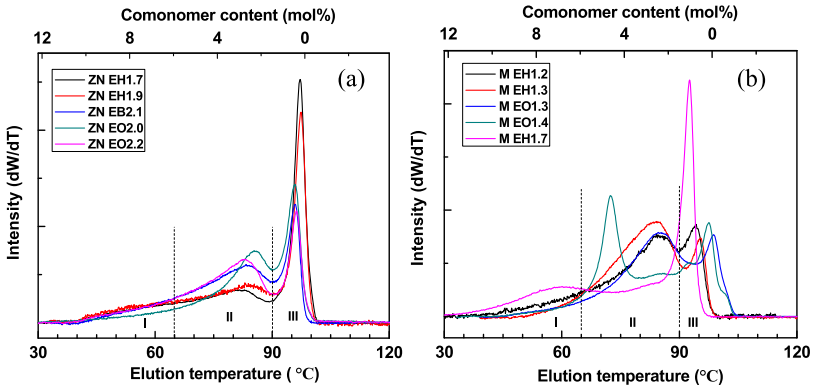

Figure 3. TREF profiles of (a) ZN-LLDPEs and (b) M-LLDPEs. Regions I, II, and III demarcate the elution range of molecules with high (12−6 mol %), medium (6−1.5 mol %), and low (<1.5 mol %) comonomer content. Elution temperatures and the corresponding comonomer contents are shown in the bottom and top x scales.

absent in Figure 1, indicating successful removal of the talc additive.[21−23] Also absent after the solution treatment are the COO− antisymmetric stretching absorbances of the carboxylate group in calcium stearate at 1540 and 1577 cm^{-1} and the ester group of Irganox at 1740 cm^{-1}, as shown in the insets of Figure 1.[24,25] Calcium stearate was present in the original spectra of ZN EO2.2, ZN EO2.0, and M EO1.3, and Irganox 1010 was present in all original samples except ZN EO2.2 and ZN EO2.0. Most ZN and metallocene LLDPEs show a small vinyl absorbance (905 cm^{-1}). ZN EH1.7 displays an absorbance at 965 cm^{-1} consistent with Trans-vinylene groups. Such absorbance becomes prominent after the removal of talc by Soxhlet extraction, as seen in Figure 1a.[26] FTIR spectra prior to and after solvent treatment are shown comparatively in the Supporting Information (Figures S3 and S4).

The comonomer composition distribution was characterized by temperature rising elution fractionation (TREF) using a TREF300 instrument commercialized by PolymerChar (Spain) with 1,2,4-trimethylbenzene as the polymer solvent and also as the solvent eluent in the column. The crystallization rate was 0.1 °C/min from the stabilization temperature of 95 °C down to 30 °C, and the subsequent solvent elution rate was 0.5 mL/min from 30 to 130 °C at a rate of 1 °C/min.

The crystallization and melting behaviors were followed by differential scanning calorimetry (DSC) using a TA Q2000 instrument and the same thermal protocols as in our previous work.[10,13] All data were collected in three continuous cycles. The heating and cooling cycles of two of these runs are schematically shown in Figure 2. As illustrated, the copolymer was first heated from 40 °C to a temperature (T_{melt}) well above the observed melting temperature of 120−125 °C, held for 5 min, and cooled to 40 °C. The heating and cooling rates were at 10 °C/min. The crystallization temperatures were read at the peak of the cooling exotherm ($T_{c,peak}$). T_{melt} was changed in a random pattern to avoid any possible systematic error in the measured crystallization temperature. As shown in Figure 2, to avoid any possible annealing of melt memory, a relatively low T_{melt}, such as 135 or 140 °C was followed by a $T_{melt} \geq 180$ °C.

Polarized optical micrographs were recorded using 50 μm thick films obtained by melt pressing the copolymer film between two microscope cover glasses. The morphology was recorded using an Olympus BX51 optical microscope equipped with an Olympus DF72 digital camera and a Linkam hot stage TMS94 for temperature control. The Linkam's stage temperature was calibrated recording the change in the light intensity of the copolymers during cooling and during heating in the polarized optical microscope, in reference to the DSC enthalpic change at the same cooling or heating rate. The morphology was followed by polarized optical microscopy using the same thermal protocols as in DSC experiments. The copolymer was heated up to a T_{melt} well above the observed melting, held for 5 min, followed by a subsequent cooling down to 40 °C, both at a rate of 10 °C/min. Micrographs of spherulites for M EH1.2 were recorded continuously (no holding time) during cooling at 10 °C/min with 1° intervals, or every 6 s.

3. RESULTS AND DISCUSSION

3.1. Characterization of Bimodal CCD. The broad bimodal comonomer composition distributions of ZN and metallocene copolymers listed in Tables 1 and 2 are first characterized by the TREF profiles shown in Figure 3a,b, respectively. The profiles are normalized by equal area and superposed to facilitate a comparative analysis. In TREF experiments, a high-temperature solution of the polymer is slowly cooled to 30 °C to separate crystallites according to the chain composition. In a subsequent step, the temperature is slowly raised while a solvent is injected and eluted at a constant flow rate.[27,28] Thinner crystals, formed from comonomer-rich molecules, dissolve and elute at the lowest temperatures, and those from the least-branched molecules elute at the highest. The concentration of eluted polymer is measured continuously, providing a CCD profile after application of a temperature−comonomer content calibration. The corresponding comonomer contents are given in the top x-axis of Figure 3. For the calibration, we used 10 comonomer composition fractions of M EH1.7, each collected within a narrow range of elution temperatures using preparative TREF in a prior work.[9] These fractions feature a narrow branching distribution as indicated by their individual TREF profiles. The comonomer content of each fraction was measured by ^{13}C NMR. The linear calibration between the mean elution temperature and comonomer content can be found in the Supporting Information (Figure S5).

To facilitate a subsequent discussion about the effect of content of branched molecules on LLPS and recrystallization from different melt temperatures, the TREF profiles are divided into three regions, demarcated by the vertical dotted lines in Figure 3a,b. Region I, ranging from an elution

https://dx.doi.org/10.1021/acs.iecr.0c03647
Ind. Eng. Chem. Res. 2020, 59, 19260−19271

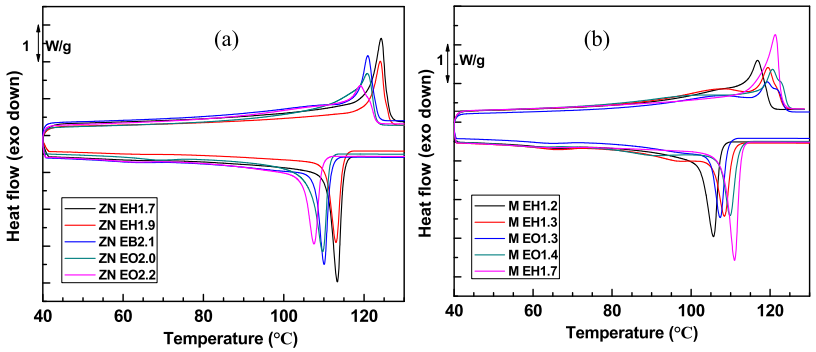

Figure 4. Crystallization from 200 °C and subsequent melting thermograms of (a) ZN-LLDPEs and (b) M-LLDPEs.

temperature of 30−65 °C, represents the highly branched molecules (comonomer content 12−6 mol %). Molecules with medium comonomer content (6−1.5 mol %) elute in Region II between 65 and ∼90 °C (85 °C for M EH1.7). Lightly branched molecules (comonomer content <1.5 mol %) are assigned to region III with a range of elution temperature from ∼90 to 105 °C.

Among the ZN-LLDPEs, copolymers ZN EH1.7 and ZN EH1.9 display relatively different TREF profiles compared to the rest of the Z-LLDPEs. These two copolymers feature a lower content of molecules in Region II (65−90 °C elution temperature) at the expense of a higher content in Region III. Furthermore, a major characteristic of copolymer ZN EO2.0 is basically a lack of highly branched molecules eluting in Region I.

The TREF profiles of M-LLDPEs shown in Figure 3b are also bimodal but mostly differ from those of the ZN-type. A major characteristic is the small content of molecules that elute in the 30−60 °C range, except for M EH1.7 that shows a relatively high content of molecules in this region. Quantitative analysis of the TREF profiles of M-LLDPEs reveals that, except for M EH1.7, the majority of the M-type copolymer molecules (∼75%) elute in Region II. Conversely, a lower content of the M-type copolymer molecules (∼25%) elutes in the high-temperature region (Region III) compared to the ZN-type, indicating a less diffuse, though still bimodal CCD in the former. M EH1.7 is an especially broad copolymer with a much higher content of the highly branched molecules. About 30% of the M EH1.7 molecules elute at temperatures <65 °C (Region I) compared to less than 10% for the rest of the M-LLDPEs studied. As seen later, this feature is important because it correlates with the extent of LLPS identified in some of the broadly distributed LLDPEs. The TREF profile of M EO1.4 is also very different from the rest. Instead of having broad components merging with Region III around 90 °C, the comonomer distribution of M EO1.4 shows two relatively narrow components, one centered at 72 °C in Region II and the other centered at ∼98 °C in Region III. Clearly, the bimodal distribution between the high and medium crystallinity components is more discrete in M EO1.4 compared to the rest, resembling the profile of a two-component mixture.[28,29]

3.2. Crystallization and Melting from Homogeneous Melts. While a slow crystallization from solution facilitates a separated crystallization of molecules by their comonomer content, thus minimizing cocrystallization, the cocrystallization of molecules with different but not too dissimilar comonomer content is unavoidable in a standard crystallization from the melt, for example, cooling at a rate of 10 °C/min.[30] Therefore, the CCD characterization of LLDPEs should be extracted from TREF profiles or by advanced TREF/GPC combination with recently introduced IR detectors.[31,32] DSC crystallization and melting thermograms may not reflect fully the double transitions expected for copolymers with bimodal CCD. Figure 4a,b displays the crystallization exotherms from a melt temperature of 200 °C and the subsequent melting endotherms of all ZN- and M-LLDPEs, respectively.

The crystallization exotherms are relatively sharp and dominated by the rapid crystallization and high enthalpic change of the lowly branched component, while the level of crystallinity and heat of fusion of molecules with a higher content of branching is much lower and spreads over a wide range of temperatures, as shown in Figure 4a,b. The final melting of a random copolymer with co-units excluded from the crystal reflects the composition of the surrounding melt. In the set of ZN-LLDPEs, the crystallization and melting peak temperatures scale proportionally with the average content of comonomer. As seen in Figure 4a and in the data listed in Table 1, ZN EH1.7 and ZN EH1.9 crystallize and melt at the highest temperatures; hence, they are expected to have a higher fraction of lowly branched molecules. In comparison, ZN EO2.2 shows the lowest values. Due to the interchain spread of comonomer composition in Regions I and II, coupled with the unavoidable cocrystallization, and the low heat of fusion of crystallites in these two regions, the endothermic transition of crystallites from molecules in these two regions is broad and overlaps with melting of the high-crystallinity fraction.

Compared with the ZN copolymers, the double melting profiles of M-LLDPEs reflect better the bimodal distribution of these copolymers (Figure 4b). The crystallization and melting of the medium and high-branched molecules of M-LLDPEs are more prominent, denoting a more discrete distribution between the high-crystallinity and low-crystallinity components, as also indicated by the TREF profiles. The double melting of the high-crystallinity component of M EO1.3 and M EO1.4 indicates a double population of molecules with little but different branching content, which also shows up in the TREF profiles of Figure 3b at ∼98 and 102 °C.

3.3. Effect of CCD on Melt Memory and LLPS. The effect of melt temperature on recrystallization was evaluated by DSC following the thermal protocol described in the experimental part and in Figure 2. A representative example is given in Figure 5 for M EO1.4. The exotherms are shown on a more expanded scale in the inset of this figure. At T_{melt} > 160 °C, the crystallization temperature does not change, indicating a homogeneous melt state. For 135 °C < T_{melt} < 160 °C, the

https://dx.doi.org/10.1021/acs.iecr.0c03647
Ind. Eng. Chem. Res. 2020, 59, 19260−19271

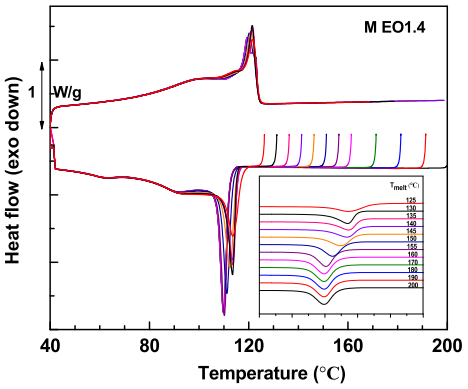

Figure 5. Plot of heat flow against temperature for cooling from melt temperatures in the range of 200−125 °C and subsequent heating for M EO1.4. Cooling and heating rates at 10 °C/min. The inset emphasizes the increase of the rate of crystallization with lowering T_{melt}.

crystallization temperature increases from 110 to 113.5 °C, reflecting a self-nucleated melt state that is no longer homogeneous. Despite drastic differences in crystallization with lowering T_{melt}, the melting endotherms are essentially unchanged, indicating that the differences in crystallization rate are due to differences in self-nucleation density, as previously discussed for model copolymers and narrow M-LLDPEs.[10,13] The remarkable feature is that the recrystallization starts to increase from any T_{melt} < 160 °C, well above the final melting of these copolymer crystals (~123 °C). In other words, clusters of ethylene sequences from the initial crystals remain in the melt and act as self-nuclei at ~40° above the observed melting. Such a large difference between the end of melting and the onset of melt memory is a unique feature of random ethylene copolymers. Comparatively, linear unbranched polyethylenes are basically free of melt memory.[10] The strong self-nucleation effect in random copolymers was mentioned in a recent review,[33] but with no emphasis on it being the largest ever reported or why self-nuclei can survive at such high melt temperatures.

Given that the emphasis of this work is on a comparative analysis between ZN and metallocene copolymers, the variation of the crystallization peak temperature ($T_{c,peak}$) as a function of the initial melt temperature (T_{melt}), for both sets of copolymers, is given in Figure 6. Avoiding overlaps for clarity, separate scales show the data for ZN EH1.7 and ZN EH1.9 in Figure 6a, and the data for M EH1.7 in Figure 6b.

All copolymers display the increase of crystallization rate for T_{melt} < ~160 °C characteristic of the melt-memory effect. Three ZN-type and one M-type LLDPE display the increase in $T_{c,peak}$ followed by a decrease in crystallization rate, which is a characteristic of liquid−liquid phase separation (LLPS). To facilitate the discussion, the data are divided into four regions. For instance, region A of ZN EB2.1 (T_{melt} ≥ 165 °C) demarcates where $T_{c,peak}$ is constant and crystallizations occur from a homogeneous, one-phase melt. In region B (165 °C < T_{melt} < 150 °C), the crystallization peak shifts to higher values indicative of a melt-memory effect from the presence of self-nuclei. As posited, in this temperature range, clusters of molten ethylene sequences from the initial crystallites remain in close proximity, increasing in number as T_{melt} decreases, and thus increase the rate of recrystallization. Region C (125 °C < T_{melt} < 150°C) is where the crystallization rate is inverted,

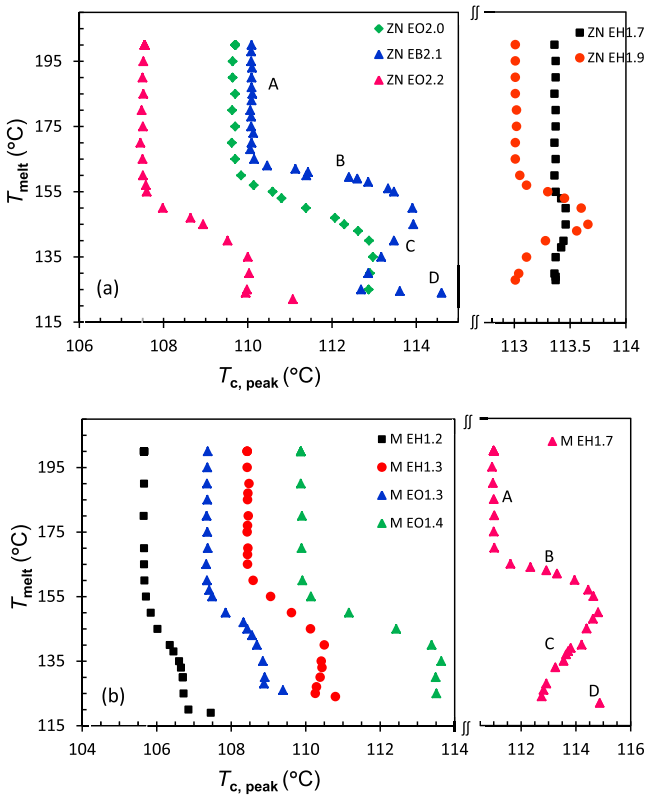

Figure 6. Temperature of the initial melt (T_{melt}) vs peak crystallization temperature ($T_{c,peak}$) for (a) ZN-LLDPEs and (b) M-LLDPEs. To avoid overlap, the data for ZN EH1.7 and ZN EH1.9 in (a) and for M EH1.7 in (b) are plotted in more expanded separated scales. The range of T_{melt} where crystallization undergoes changes is denoted as A, B, C, and D regions.

decreasing with decreasing T_{melt} instead of increasing further as expected from the melt-memory effect. This inversion of the recrystallization rate is a peculiar feature associated with LLPS, which has been observed in other broadly distributed copolymers.[13−16,34] As we showed by direct analysis of the melt using small-angle neutron scattering (SANS)[14,15] and light scattering (SALS),[15] the inversion demarcates the onset of LLPS. Lastly, Region D corresponds to relatively low T_{melt}, very close to or at the end of the observed melting peak, where a small fraction of crystals remain unmolten and serve as true self-seeds to accelerate recrystallization. As seen in Figure 6a, in region D, $T_{c,peak}$ increases again as expected. Only regions A, B, and D are present in copolymers that display melt memory but not the features of LLPS.

Since all copolymers studied have a broad comonomer distribution that spans between ~12 and 0 mol % comonomer content, the unexpected decrease of the crystallization temperature in region C in four copolymers (ZN EH1.7, ZN EH1.9, ZN EB2.1, and M EH1.7) must be related to the differences in the uneven contents of molecules across the broad CCD.[13,16] During the initial relatively fast cooling from a homogeneous melt, cocrystallization of sequences from molecules of different comonomer content is unavoidable in copolymers with progressive change in composition in a broad range, such as the copolymers analyzed here. It is likely that sequences in Region I cocrystallize with sequences of Region II (by forming part of the same lamellae crystal). Similarly, sequences in Region II will likely cocrystallize with sequences in Region III, but due to the large differences in crystallization

https://dx.doi.org/10.1021/acs.iecr.0c03647
Ind. Eng. Chem. Res. 2020, 59, 19260−19271

kinetics, it is unlikely that sequences of Regions I and III cocrystallize. It is known from early works that blends of ethylene copolymers with a difference in comonomer content >8 mol % phase-separate in the melt.[19,35−38] The phase diagram shows an upper critical solution temperature (UCST) at ∼150 °C, which is the temperature between regions B and C in Figure 6.[39−42] When the crystals are brought to a T_{melt} in region C, below the UCST, clusters from cocrystals between molecules of Regions III and II most probably survive as the difference in comonomer content is <8 mol %. However, clusters from cocrystals of molecules in Regions II and I (>8 mol % difference in comonomer content) do not survive as the strong thermodynamic drive for phase separation dissolves them. The comonomer-rich and comonomer-poor molecules diffuse to their LLPS domains, and in this path, they drag their ethylene segments away from the cluster. The recrystallization rate decreases in this region because the drive to phase separation is stronger when T_{melt} is further below the UCST.

Copolymers ZN EH1.7, ZN EH1.9, ZN EB2.1, and M EH1.7 show the characteristic inversion of $T_{c,peak}$ due to the interplay between melt memory and LLPS. The other two ZN copolymers analyzed, ZN EO2.0 and ZN EO2.2, display a large extent of melt memory, up to 3.5 °C increase in $T_{c,peak}$ for ZN EO2.0, but no inversion of crystallization rate despite the broad CCD (Figure 6a).

As shown in Figure 6b, all M-LLDPEs display the shift of $T_{c,peak}$ to higher values at a critical high T_{melt} consistent with the onset of melt memory. However, except M EH1.7, none display the inversion of the crystallization rate associated with LLPS. Since the major difference between M EH1.7 and the rest of the metallocene copolymers is the content of molecules in Regions I and II, it is obvious that a specific CCD with a critical content of molecules in these regions is needed to first allow cocrystallization of compositionally differing molecules during the cooling step, and further dissolution of some clusters when reaching LLPS at T_{melt} ∼ 150 °C.

To quantify the effects of melt memory and LLPS on crystallization, we introduce two parameters as illustrated in Figure 7. The extent of melt memory, which reflects the maximum number of self-nuclei (ethylene clusters), is defined as the largest difference in $T_{c,peak}$ within region B. The extent of LLPS indicates the loss of self-nuclei in the temperature range of the phase-separated melt and is taken as the largest difference in $T_{c,peak}$ within region C. Furthermore, T_{onset} demarcates the onset of melt memory reflecting homogeneous melts at any $T_{melt} > T_{onset}$. T_{LLPS} infers the upper critical temperature of melt phase separation. Table 3 summarizes the extent of melt memory, the extent of LLPS, T_{onset}, and T_{LLPS} for all of the copolymers studied.

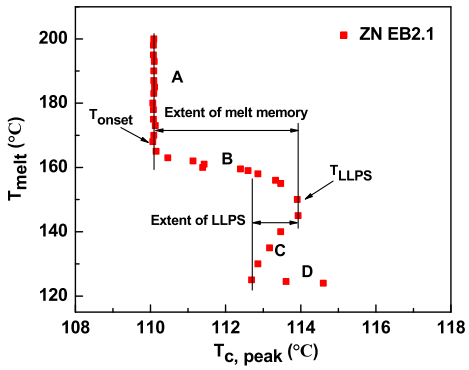

Figure 7. Variation of $T_{c,peak}$ (x-axis) as a function of T_{melt} (y-axis) for ZN EB2.1 to illustrate the parameters associated with melt memory and LLPS. Shown are the onset of melt memory (T_{onset}), extent of melt memory, onset of LLPS (T_{LLPS}), and extent of LLPS.

The contents of molecules with high, medium, and low comonomer content, given by the areas beneath Regions I, II, and III of the TREF profiles of Figure 3, are listed in Table 3. Also included is the range of comonomer content in each region. We focus on Regions I and II as they contribute the most to LLPS. Copolymers that show the inversion of crystallization rate, and thus give evidence of LLPS, have a content of molecules in Region I (12−6 mol % comonomer) ≥15 wt % and have <∼50 wt % molecules in Region II (6−1.5 mol % comonomer). The low comonomer content (<1.5 mol %) comprises 30−50 wt % molecules. The only exception is ZN EO2.2 that displays a TREF profile almost identical to ZN EB2.1 but does not have evidence of LLPS. We can only speculate that the longer branch of ethylene 1-octenes may slow down diffusion, and much longer time in the melt will be needed to dissolve clusters from the cocrystals in ethylene 1-octene copolymers.

The only M-LLDPE that shows evidence of LLPS is M EH1.7 with CCD distribution that falls under the requirements observed for ZN copolymers with LLPS. M EH1.7 shows 26 wt % molecules in Region I (>15 wt %), 27 wt % in Region II (<50 wt %), and 47 wt % in Region III. While the distribution is also broad in the rest of the M-LLDPEs studied, the content of molecules in Region I is <7 wt %; hence, they lack a sufficient number of highly branched molecules (>8 mol % comonomer) to enable the characteristic inversion of crystallization rate associated with LLPS. For those M-LLDPEs that do not show LLPS, a lower content of molecules in Region I is compensated by a higher content in Region II. The inversion of the recrystallization temperature is a very sensitive probe for LLPS in broad LLDPEs, even if they form very small phase-separated domains that are difficult to identify by high-resolution microscopy.[13]

From the data of Table 3 and Figure 6, we conclude that melt memory and a subsequent inversion of the crystallization rate due to the advent of LLPS is manifested at the greatest extent in broad copolymers with 15−25 wt % molecules in a range of comonomer composition between 12 and 6 mol % (Region I), a content of 30−50 wt % in a composition range of 6−1.5 mol % (Region II), and with 40−50 wt % molecules of <1.5 mol % comonomer (Region III).

The content of molecules in each region is plotted against the extent of melt memory for ZN- and M-LLDPEs in Figures 8a,b, respectively. For both types of copolymers, the extent of melt memory increases with increasing content of molecules in Region II and with decreasing content in Region III. These results are consistent with previous data obtained in narrowly distributed copolymers, which indicated stronger melt memory in copolymers with 2−6 mol % comonomer (1−3 mol % branches). In fact, a bell shape with maximum at 1.5−2 mol % branches is found for the strength of melt memory with increasing comonomer content in narrow copolymers.[13] At the highest comonomer content, melt memory is low because the level of crystallinity is insufficient to build the constraints required in the amorphous regions. Conversely, molecules with none or low content of branches lack the sequence selection process during crystallization that leads to the topological constraints, responsible for the strong memory observed in

https://dx.doi.org/10.1021/acs.iecr.0c03647
Ind. Eng. Chem. Res. 2020, 59, 19260−19271

Table 3. Content of Molecules (wt %) and Average Comonomer Composition (mol %) in Regions I, II, and III of the TREF Profiles of ZN-LLDPEs and M-LLDPEs[a]

sample ID	content (wt %) Region I (13−6 mol % comonomer)	content (wt %) Region II (6−1.5 mol % comonomer)	content (wt %) Region III (<1.5 mol % comonomer)	extent of melt memory (°C)	extent of LLPS (°C)	T_{onset} (°C)	T_{LLPS} (°C)
ZN EH1.7	15.0 (7.7)	33.0 (3.7)	52.0 (0.3)	0.1	0.1	157	150
ZN EH1.9	17.3 (7.7)	38.9 (3.5)	43.8 (0.3)	0.7	0.7	162	145
ZN EB2.1	15.6 (7.5)	55.8 (3.5)	28.6 (0.6)	3.8	1.2	165	150
ZN EO2.2	15.9 (7.6)	57.4 (3.5)	26.7 (0.5)	2.5		160	
ZN EO2.0	8.4 (7.6)	53.2 (3.1)	38.4 (0.6)	3.3		165	
M EH1.2	10.2 (7.5)	63.3 (3.3)	26.5 (0.9)	1.1		160	
M EH1.3	6.6 (7.0)	77.0 (3.3)	16.4 (0.6)	2.1		165	
M EO1.3	6.6 (7.2)	70.1 (2.9)	23.4 (0.01)	1.6		160	
M EO1.4	7.0 (6.8)	70.0 (3.6)	23.0 (0.1)	3.7		160	
M EH1.7	26.0 (8.1)	27.0 (4.0)	47.0 (1.2)	3.8	2.0	168	150

[a]The extent of melt memory, extent of LLPS, and critical temperatures of melts associated with melt memory (T_{onset}) and LLPS (T_{LLPS}) are also listed.

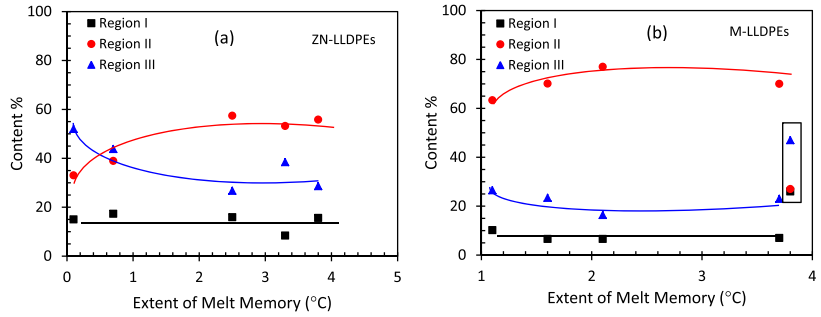

Figure 8. Content of molecules in Regions I, II, and III of the CCD distribution of broad ethylene copolymers vs extent (width) of melt memory. (a) ZN-LLDPEs and (b) M-LLDPEs. The open vertical rectangle highlights the data for M EH1.7.

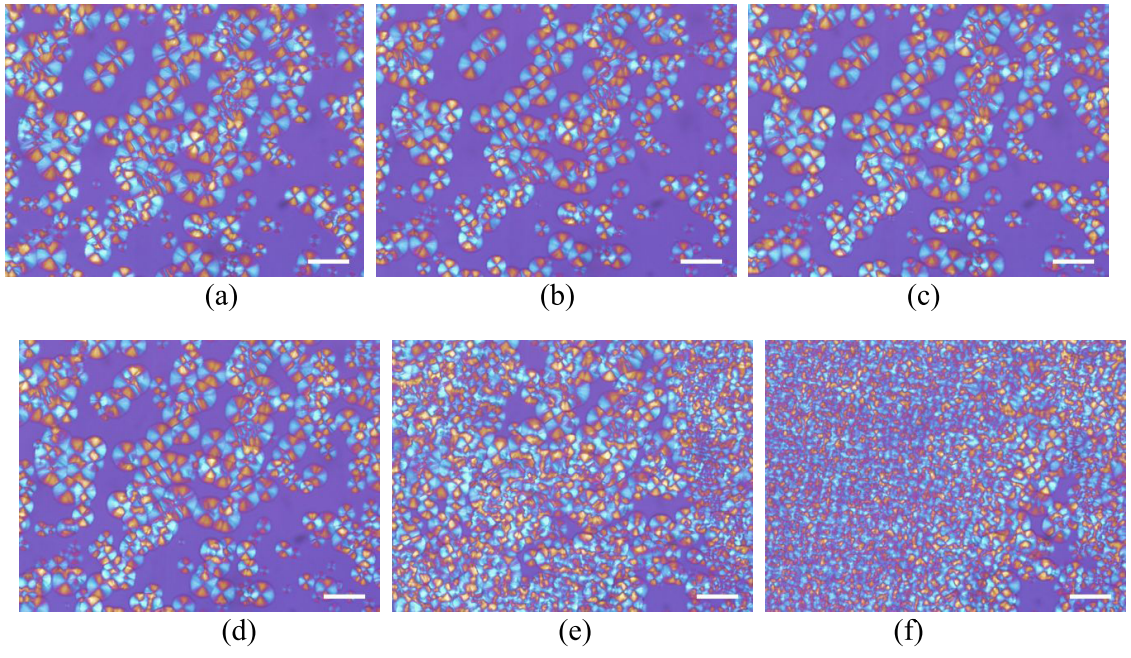

Figure 9. Optical micrographs taken at 106 °C for M EH1.2 crystallized during cooling from a T_{melt} of (a) 200, (b) 160, (c) 150, (d) 145, (e) 130, and (f) 125 °C. The thermal sequence on each micrograph was (200−40−T_{melt}−106 °C). The scale bar represents a length of 50 μm.

more branched random copolymers. In Figure 8b, the highlighted data for M EH1.7 do not follow the trend of the other copolymers. It appears that the distribution of copolymer molecules between Regions II and III in M EH1.7 (see Figure 3b) favors cocrystallization of molecules that comprise these two regions, assisting with the stability of self-nuclei and leading to a larger extent of melt memory up to the onset of LLPS.

3.4. Morphological Evidence of Melt Memory and LLPS. The signature of the melt memory-increasing recrystallization temperature is evident from the DSC data in all copolymers analyzed in this and prior works. However, due to

https://dx.doi.org/10.1021/acs.iecr.0c03647
Ind. Eng. Chem. Res. 2020, 59, 19260−19271

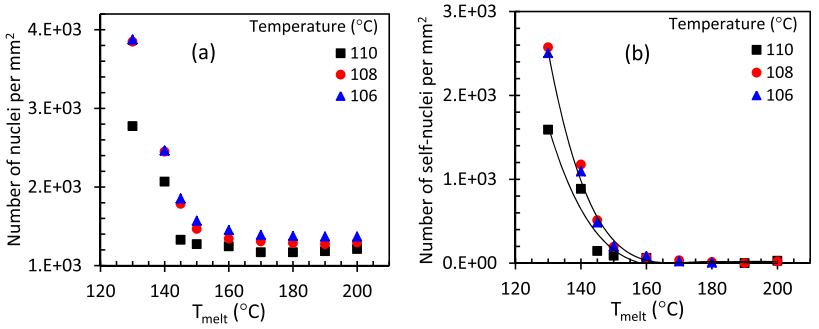

Figure 10. (a) Number of nuclei (heterogeneous and self-nuclei) at temperatures of 106, 108, and 110 °C on cooling from different T_{melt} for M EH1.2 (cooling rate: 10 °C/min). (b) Number of self-nuclei vs T_{melt}. The solid lines represent exponential fittings.

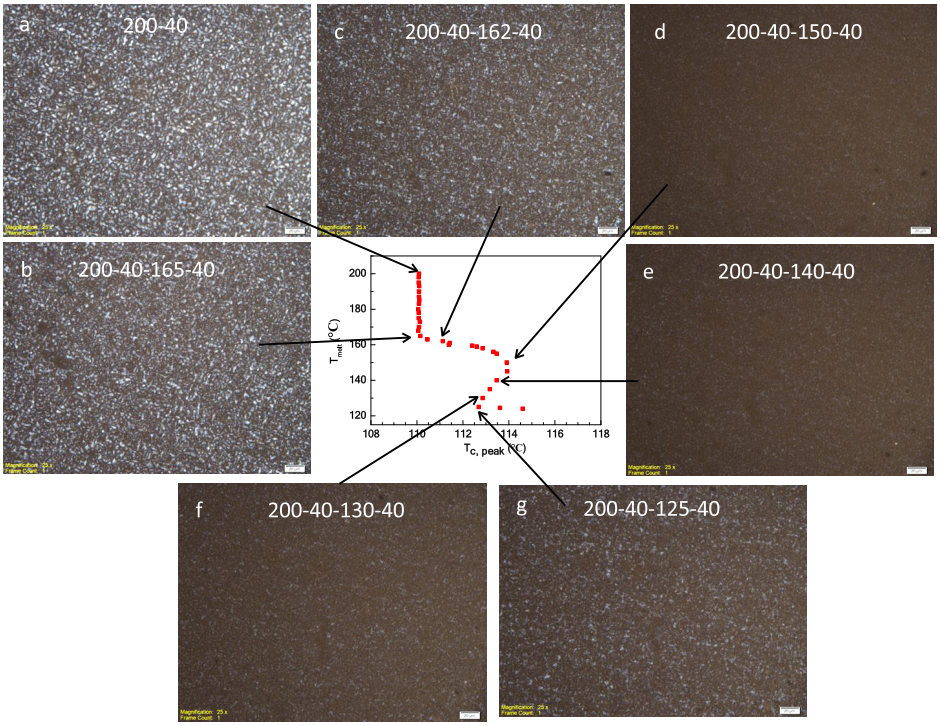

Figure 11. Optical micrographs taken at 40 °C for ZN EB2.1 crystallized during cooling from a T_{melt} of (a) 200, (b) 165, (c) 162, (d) 150, (e) 140, (f) 130, and (g) 125 °C. As shown by the thermal sequence on each micrograph (200−40−T_{melt}−40), T_{melt} was reached from 40 °C. The scale bar represents a length of 20 μm.

the very high nucleation density, the morphological evidence given in earlier work was only qualitative.[10,13,15,16] Of the systems studied in the present work, M EH1.2 is an experimental resin free of the additives usually found in commercial LLDPEs. Due to a cleaner synthetic path, M EH1.2 resulted with a comparatively small number of heterogeneities, and the number of self-nuclei active in the range of melt memory could be quantitatively determined in this resin independently of the heterogeneous nuclei.

The thermal protocol followed was identical to the one used to obtain the data of Figure 6. The standard semicrystalline state formed by cooling from 200 to 40 °C was heated to a specific T_{melt} and then cooled at 10 °C/min. Images were taken during the cooling process from different T_{melt}. A representative set of micrographs taken at 106 °C during cooling from different T_{melt} covering the range of crystallization of copolymer M EH1.2 from homogeneous and self-nucleated melts is given in Figure 9. As shown in the DSC exotherms of Figure 4, 106 °C corresponds to a relatively fast stage of crystallization of M EH1.2. The number of spherulites, or number of nuclei, is unchanged in the images of Figure 9a,b, thus indicating constant nucleation density for crystallizations from the homogeneous melt ($T_{melt} \geq 160$ °C). As T_{melt} decreases further, the number of spherulites that develop at 106 °C first increases slowly (Figure 9c,d) and for $T_{melt} \leq 145$ °C increases rapidly, leading to finer morphologies indicative of a very rapid increase in the number of nuclei (Figure 9e−f).

The number of nuclei per unit area is plotted as a function of T_{melt} in Figure 10a for micrographs recorded when the temperature reached 110, 108, or 106 °C during cooling from different T_{melt}. As shown, for $T_{melt} > 160$ °C, the number of nuclei is constant with a small variation at any fixed T_{melt}. These constant nuclei reflect the number of heterogeneous nuclei (other than those from the copolymer molecules) encountered in any semicrystalline polymer.[33,43] It is obvious in Figure 9 that the spherulites develop from heterogeneous nuclei at $T_{melt} \geq 160$ °C because they appear in the same location. As T_{melt} decreases below 160 °C, thus crossing the

https://dx.doi.org/10.1021/acs.iecr.0c03647
Ind. Eng. Chem. Res. 2020, 59, 19260−19271

onset T_{melt} for melt memory (see Figure 6), the number of nuclei starts to increase slowly first, and then very rapidly, until counting becomes impossible for T_{melt} < 125 °C. The difference between the number of nuclei at T_{melt} < 160 °C and the constant number for T_{melt} > 160 °C are the number of self-nuclei or clusters of ethylene sequences that remain at T_{melt} < T_{onset}. As shown in Figure 10b, the number of self-nuclei is 0 at T_{melt} ≥ 160 °C and increases exponentially for recrystallizations from lower T_{melt}. The images in Figure 9, and the data in Figure 10, provide the first quantitative direct evidence of self-nuclei that increase the recrystallization rate of LLDPEs.

While, as mentioned earlier, quantitative accounts of self-nuclei could only be recorded for one copolymer, the effect of the number of nuclei that remain at any T_{melt} can also be observed in the overall spherulitic morphology of all copolymers, including the dissolution of self-nuclei at T_{melts} entering the LLPS region. An example is given by the composite of DSC data and polarized optical micrographs for copolymer ZN EB2.1 in Figure 11. The micrographs were taken in black and white to emphasize the contrast. All micrographs were obtained at 40 °C after cooling from the indicated T_{melt}. The morphology is coarse when recrystallization is from T_{melt} > 165 °C, indicating that only heterogeneous nuclei remain in this range of temperatures and the copolymer melt is homogeneous (images a and b in Figure 11). In the range of T_{melt} between the onset of melt memory and the onset of LLPS, the spherulitic morphology becomes finer, indicating that in addition to the heterogeneous nuclei there are self-nuclei from the initial crystalline ethylene sequences. A much higher number of nuclei lead to smaller crystals and a darker appearance of the overall micrographs as seen in images (c) and (d) of Figure 11. In the LLPS region, some self-nuclei are dissolved; consequently, the morphology becomes a little coarser and brighter for T_{melt} between 150 and 125 °C. The same morphological changes are seen in the rest of the copolymers that show the inversion in the recrystallization rate. Copolymers with no LLPS display the features seen in the micrographs of Figure 11a−d.

4. CONCLUSIONS

The effect of crystalline memory in melts of LLDPE on recrystallization was comparatively studied in a series of copolymers synthesized with Ziegler−Natta (ZN) or metallocene (M) catalysts. The copolymers have the same M_w, the same polydispersity, similar average comonomer content, and different broad-bimodal comonomer composition distribution (CCD). The characteristics of the recrystallization depend strongly on the profiles of the CCD.

All ZN- and M-LLDPEs display the enhanced recrystallization due to melt memory when cooled from T_{melt} below a critical temperature that for these copolymers is >40 °C above the observed melting point.

For most ZN-LLDPEs, the enhanced recrystallization is followed by a retardation, or inversion of the rate at T_{melt} < 150 °C. The inversion demarcates the onset of LLPS with dissolution of some clusters (self-nuclei) during the thermodynamic phase separation process. Conversely, most M-LLDPEs studied do not show the retardation of crystallization features associated with LLPS.

A quantitative evaluation of TREF profiles allows us to conclude that the rate-inversion signature of LLPS requires ZN or M copolymers with 15−25 wt % molecules in the 12−6 mol % comonomer composition range, and <∼50 wt % in a range of 6−1.5 mol % comonomer. The rest of the lowly branched molecules (<1.5 mol % comonomer) comprise the high-crystallinity component of the copolymer (30−50 wt %).

The effect of self-nucleated melts at different levels on the overall spherulitic morphology is documented via polarized optical microscopy. For the first time, we obtained independent quantitative data for the numbers of heterogeneous and self-nuclei in random ethylene copolymers. The data suggest an exponential variation of self-nuclei with decreasing T_{melt}.

The comparative CCD-crystallization analysis carried out in this work serves as a guideline to design LLDPEs with distributions prone to LLPS during processing. While the effect of melt memory on enhancing the recrystallization rate may be beneficial to optimize postprocessing technologies, the advent of LLPS identified by DSC may lead to a simple route to predict the superior impact properties of these materials.

■ ASSOCIATED CONTENT

Supporting Information

The Supporting Information is available free of charge at https://pubs.acs.org/doi/10.1021/acs.iecr.0c03647.

GPC profiles of ZN- and M-LLDPEs, GPC profiles of original and solvent-treated ZN EB2.1, comparative FTIR spectra of original and solvent-treated LLDPEs, and comonomer content—TREF elution temperature calibration for LLDPEs (PDF)

■ AUTHOR INFORMATION

Corresponding Author

Rufina G. Alamo − *Department of Chemical and Biomedical Engineering, FAMU/FSU College of Engineering, Tallahassee, Florida 32310, United States;* orcid.org/0000-0002-3061-499X; Email: alamo@eng.fsu.edu

Authors

Minqiao Ren − *Department of Chemical and Biomedical Engineering, FAMU/FSU College of Engineering, Tallahassee, Florida 32310, United States*

Xuejian Chen − *Department of Chemical and Biomedical Engineering, FAMU/FSU College of Engineering, Tallahassee, Florida 32310, United States*

Yuan Sang − *Department of Chemical and Biomedical Engineering, FAMU/FSU College of Engineering, Tallahassee, Florida 32310, United States*

Complete contact information is available at: https://pubs.acs.org/10.1021/acs.iecr.0c03647

Notes

The authors declare no competing financial interest.

■ ACKNOWLEDGMENTS

This work is based on the work supported by the USA National Science Foundation (DMR 1607786). The authors also acknowledge David Fiscus from ExxonMobil, and Gang Zheng, Meifang Guo, Honghong Huang, and Dong Wei of SINOPEC Beijing Research Institute of Chemical Industry for samples and TREF and GPC measurements.

REFERENCES

(1) Brintzinger, H. H.; Fischer, D.; Mülhaupt, R.; Rieger, B.; Waymouth, R. M. Stereospecific Olefin Polymerization with Chiral Metallocene Catalysts. *Angew. Chem., Int. Ed. Engl.* **1995**, *34*, 1143−1170.

(2) Chum, P. S.; Swogger, K. W. Olefin Polymer Technologies—History and Recent Progress at The Dow Chemical Company. *Prog. Polym. Sci.* **2008**, *33*, 797−819.

(3) Hubert, L.; Vigier, G.; Degoulet, C.; Germain, Y.; et al. Physical and Mechanical Properties of Polyethylene for Pipes in Relation to Molecular Architecture. I. Microstructure and Crystallisation Kinetics. *Polymer* **2001**, *42*, 8425−8434.

(4) Liu, H.-T.; Davery, C. R.; Shirodkar, P. P. Bimodal Polyethylene Products from UNIPOLTM Single Gas Phase Reactor Using Engineered Catalysts. *Macromol. Symp.* **2003**, *195*, 309−316.

(5) Anantawaraskul, S.; Soares, J. B. P.; Wood-Adams, P. M. Fractionation of Semicrystalline Polymers by Crystallization Analysis Fractionation and Temperature Rising Elution Fractionation. *Adv. Polym. Sci.* **2005**, *182*, 1−54.

(6) Krishnaswamy, R. K.; Yang, Q.; Fernandez-Ballester, L.; Kornfield, J. A. Effect of the Distribution of Short-Chain Branches on Crystallization Kinetics and Mechanical Properties of High-Density Polyethylene. *Macromolecules* **2008**, *41*, 1693−1704.

(7) Alamo, R. G.; Blanco, J. A.; Agarwal, P. K.; Randall, J. C. Crystallization Rates of Matched Fractions of MgCl 2 -Supported Ziegler Natta and Metallocene Isotactic Poly(Propylene)s. 1. The Role of Chain Microstructure. *Macromolecules* **2003**, *36*, 1559−1571.

(8) Randall, J. C.; Alamo, R. G.; Agarwal, P. K.; Ruff, C. J. Crystallization Rates of Matched Fractions of MgCl 2 -Supported Ziegler-Natta and Metallocene Isotactic Poly(Propylene)s. 2. Chain Microstructures from a Supercritical Fluid Fractionation of a MgCl2-Supported Ziegler-Natta Isotactic Poly(Propylene). *Macromolecules* **2003**, *36*, 1572−1584.

(9) Vadlamudi, M.; Subramanian, G.; Shanbhag, S.; Alamo, R. G.; Fiscus, D. M.; Brown, G. M.; Lu, C.; Ruff, C. J.; et al. Molecular Weight and Branching Distribution of a High Performance Metallocene Ethylene 1-Hexene Copolymer Film-Grade Resin. *Macromol. Symp.* **2009**, *282*, 1−13.

(10) Reid, B. O.; Vadlamudi, M.; Mamun, A.; Janani, H.; Gao, H.; Hu, W.; Alamo, G. Strong Memory Effect of Crystallization above the Equilibrium Melting Point of Random Copolymers. *Macromolecules* **2013**, *46*, 6485−6497.

(11) Gao, H.; Vadlamudi, M.; Alamo, R. G.; Hu, W. Monte Carlo Simulations of Strong Memory Effect of Crystallization in Random Copolymers. *Macromolecules* **2013**, *46*, 6498−6506.

(12) Chen, X.; Mamun, A.; Alamo, R. G. Effect of Level of Crystallinity on Melt Memory above the Equilibrium Melting Temperature in a Random Ethylene 1-Butene Copolymer. *Macromol. Chem. Phys.* **2015**, *216*, 1220−1226.

(13) Mamun, A.; Chen, X.; Alamo, R. G. Interplay between a Strong Memory Effect of Crystallization and Liquid-Liquid Phase Separation in Melts of Broadly Distributed Ethylene-1-Alkene Copolymers. *Macromolecules* **2014**, *47*, 7958−7970.

(14) Chen, X.; Wignall, G. D.; He, L.; Lopez-Barron, C.; Alamo, R. G. SANS Evidence of Liquid-Liquid Phase Separation Leading to Inversion of Crystallization Rate of Broadly Distributed Random Ethylene Copolymers. *Macromolecules* **2017**, *50*, 4406−4414.

(15) Chen, X.; López-Barrón, C.; Zeng, Y.; Alamo, R. G. Concentration Fluctuations in the Early Stages of LLPS and Partial Dissolution of Melt-Memory in Broadly Distributed Ethylene Copolymers. *Polymer* **2018**, *148*, 181−190.

(16) Ren, M.; Chen, X.; Sang, Y.; Alamo, R. G. Effect of Heterogeneous Short Chain Branching Distribution on Acceleration or Retardation of the Rate of Crystallization from Melts of Ethylene Copolymers Synthesized with Ziegler-Natta Catalysts. *Macromol. Symp.* **2015**, *356*, 131−141.

(17) Chen, X.; Qu, C.; Alamo, R. G. "Effect of Annealing Time and Molecular Weight on Melt Memory of Random Ethylene 1-Butene Copolymers". *Polym. Int.* **2019**, *68*, 248−256.

(18) Marxsen, S. F.; Alamo, G. Melt-Memory of Polyethylenes with Halogen Substitution: Random vs. Precise Placement. *Polymer* **2019**, *168*, 168−177.

(19) Wignall, G. D.; Alamo, R. G.; Ritchson, E. J.; Mandelkern, L.; Schwahn, D. SANS Studies of Liquid-Liquid Phase Separation in Heterogeneous and Metallocene-Based Linear Low-Density Polyethylenes. *Macromolecules* **2001**, *34*, 8160−8165.

(20) Randall, J. C. A Review of High Resolution Liquid 13Carbon Nuclear Magnetic Resonance Characterizations of Ethylene-Based Polymers. *J. Macromol. Sci., Rev. Macromol. Chem. Phys.* **1989**, *29*, 201−317.

(21) De Medeiros, E. S.; Tocchetto, R. S.; De Carvalho, L. H.; Santos, I. M. G.; Souza, A. G. Nucleating Effect and Dynamic Crystallization of a Poly (propylene)/talc System. *J. Therm. Anal. Calorim.* **2001**, *66*, 523−531.

(22) Naiki, M.; Fukui, Y.; Matsumura, T.; Nomura, T.; Matsuda, M. The Effect of Talc on the Crystallization of Isotactic Polypropylene. *J. Appl. Polym. Sci.* **2001**, *79*, 1693−1703.

(23) Castillo, L. A.; Barbosa, S. E.; Capiati, N. J. Influence of Talc Genesis and Particle Surface on the Crystallization Kinetics of Polypropylene/Talc Composites. *J. Appl. Polym. Sci.* **2012**, *126*, 1763−1772.

(24) Deamer, D. W.; Meek, D. W.; Cornwell, D. G. Properties, composition, and structure of stearic acid-stearate monolayers on alkaline earth solutions. *J. Lipid Res.* **1967**, *8*, 255−263.

(25) Krimm, S.; Liang, C. Y.; Sutherland, G. B. B. M. Infrared Spectra of High Polymers. II. Polyethylene. *J. Chem. Phys.* **1956**, *25*, 549−562.

(26) Bracco, P.; Brunella, V.; Luda, M. P.; Zanetti, M.; Costa, L. Radiation-Induced Crosslinking of UHMWPE in the Presence of Co-Agents: Chemical and Mechanical Characterisation. *Polymer* **2005**, *46*, 10648−10657.

(27) Francuskiewicz, F. Temperature Rising Elution Fractionation. In *Polymer Fractionation*; Springer: Berlin, Heidelberg, 1994; pp 137−144.

(28) Monrabal, B. Temperature Rising Elution Fractionation and Crystallization Analysis Fractionation. In *Encyclopedia of Analytical Chemistry*; Wiley: Chichester, UK, 2000; pp 8074−8094.

(29) Mirabella, F. M.; Ford, E. A. Characterization of Linear Low-Density Polyethylene: Cross-Fractionation According to Copolymer Composition and Molecular Weight. *J. Polym. Sci., Part B: Polym. Phys.* **1987**, *25*, 777−790.

(30) Galante, M. J.; Mandelkern, L.; Alamo, R. G. The Crystallization of Blends of Different Type Polyethylenes: The Role of Crystallization Conditions. *Polymer* **1998**, *39*, 5105−5119.

(31) Ortin, A.; Monrabal, B.; Sancho-tello, J. Development of an Automated Cross-Fractionation Apparatus (TREF-GPC) for a Full Characterization of the Bivariate Distribution of Polyolefins. *Macromol. Symp.* **2007**, *257*, 13−28.

(32) Monrabal, B. Polyolefin Characterization: Recent Advances in Separation Techniques. *Adv. Polym. Sci.* **2013**, *257*, 203−251.

(33) Sangroniz, L.; Cavallo, D.; Mu, A. J. Self-Nucleation Effects on Polymer Crystallization. *Macromolecules* **2020**, *53*, 4581−4604.

(34) Ren, M.; Tang, Y.; Gao, D.; Ren, Y.; Yao, X.; Shi, H.; Zhang, T.; Wu, C. Recrystallization of Biaxially Oriented Polyethylene Film from Partially Melted State within Crystallite Networks. *Polymer* **2020**, *191*, No. 122291.

(35) Alamo, R. G.; Graessley, W. W.; Krishnamoorti, R.; Lohse, D. J.; Londono, J. D.; Mandelkern, L.; Stehling, F. C.; Wignall, G. D. Small Angle Neutron Scattering Investigations of Melt Miscibility and Phase Segregation in Blends of Linear and Branched Polyethylenes as a Function of the Branch Content. *Macromolecules* **1997**, *30*, 561−566.

(36) Mandelkern, L.; Alamo, R. G.; Wignall, G. D.; Stehling, F. C. The phase structure of blends of the different polyethylenes. *Trends Polym. Sci.* **1996**, *4*, 377−383.

(37) Wignall, G. D.; Alamo, R. G.; Londono, J. D.; Mandelkern, L.; Kim, M. H.; Lin, J. S.; Brown, G. M. Morphology of Blends of Linear and Short-Chain Branched Polyethylenes in the Solid State by Small-

https://dx.doi.org/10.1021/acs.iecr.0c03647
Ind. Eng. Chem. Res. 2020, 59, 19260−19271

Angle Neutron and X-Ray Scattering, Differential Scanning Calorimetry, and Transmission Electron Microscopy. *Macromolecules* **2000**, *33*, 551−561.
(38) Crist, B.; Nesarikar, A. R. Coarsening in Polyethylene-Copolymer Blends. *Macromolecules* **1995**, *28*, 890−896.
(39) Wang, H.; Shimizu, K.; Hobbie, E. K.; Wang, Z.; Meredith, J. C.; Karim, A.; Amis, E. J.; Hsiao, B. S.; Hsieh, E. T.; Han, C. C. Phase Diagram of a Nearly Isorefractive Polyolefin Blend. *Macromolecules* **2002**, *35*, 1072−1078.
(40) Wang, H.; Shimizu, K.; Kim, H.; Hobbie, E. K.; Wang, Z.; Han, C. C. Competing Growth Kinetics in Simultaneously Crystallizing and Phase-Separating Polymer Blends. *J. Chem. Phys.* **2002**, *116*, 7311−7315.
(41) Zhang, X.; Wang, Z.; Han, C. C. Fine Structures in Phase-Separated Domains of a Polyolefin Blend via Spinodal Decomposition. *Macromolecules* **2006**, *39*, 7441−7445.
(42) Shimizu, K.; Wang, H.; Matsuba, G.; Wang, Z.; Kim, H.; Peng, W.; Han, C. C. Interplay of Crystallization and Liquid-Liquid Phase Separation in Polyolefin Blends: A Thermal History Dependence Study. *Polymer* **2007**, *48*, 4226−4234.
(43) Massa, M. V.; Carvalho, J. L.; Dalnoki-Veress, K. Direct Visualisation of Homogeneous and Heterogeneous Crystallisation in an Ensemble of Confined Domains of Poly (Ethylene Oxide). *Eur. Phys. J. E* **2003**, *12*, 111−117.

https://dx.doi.org/10.1021/acs.iecr.0c03647
Ind. Eng. Chem. Res. 2020, 59, 19260−19271